On the optical potential method as a generalized scheme to locate molecular resonances: Calculation of Feshbach resonances in the electronically elastic $H^+ + O_2$ collision.

Ken Museth*

Department of Chemistry, H.C.Ørsted Institute, University of Copenhagen, DK-2100 Copenhagen Ø, Denmark

Claude Leforestier

Laboratoire Structure et Dynamique Moléculaires, CC 014, Université des Sciences et Techniques du Languedoc, 34095 Montpellier Cédex 05, France

Danielle Grimbert

Université de Cergy-Pontoise, Pôle Sciences & Techniques, 49 av. des Genottes-BP 8428, 95806 Cergy-Pontoise Cédex, France

Victor Sidis

Laboratorie des Collisions Atomiques et Moléculaires, Université Paris-Sud XI, 91405 Orsay Cédex, France

To be submitted to Journal of Chemical Physics (Febuary 28,1997)

Running Title : Resonances in the elastic $H^+ + O_2$ collision

---

*Corresponding author

The optical potential method is reviewed here with special emphasis on the available techniques used to isolate and verify molecular resonances. We next present calculations of Feshbach resonances in the framework of the Infinite-Order Sudden approximation of the electronically elastic $H^+ + O_2$ collision. In this approximation the relative angle between the oxygen molecule and the incoming proton is kept fixed thereby reducing the problem to a two dimensional one. The investigated energy domain of the resonances is below the channel energy for the first vibrational excitation (0.2 eV). The optical potential method, used to characterize the resonances, applies a negative imaginary potential (NIP) in the asymptotic region of the electronic potential energy surface. The positions and widths of the resonances are given as respectively the real and imaginary part of the stationary complex energies with respect to variations of the amplitude of the NIP. The overall numerical scheme is an optimized discrete variable representation of the complex integrals involved. The calculated resonances are finally compared to previous two dimensional calculations obtained by Grimbert *et al.*, Chem. Phys. Lett. **230**,(1994), p. 47-53.

I. INTRODUCTION

When colliding particles temporarily stick together to form complexes we have what is known as a "resonance state" in the time-independent picture. This is a state of the system that has enough energy to break up into smaller parts as e.g. in indirect photodissociation. The formation of such resonances owes to the existence of an attractive well in the interaction potential, and ion-molecule systems like $H^+ + O_2$ are good candidates for this. Quantum mechanically, we distinguish between two different kinds of resonances owing to the underlying mechanisms. The simplest are the so-called *shape* or elastic resonances where the wave function is trapped in the well behind a barrier. As illustrated in Fig. 1 this could be the result of an non-adiabatic coupling between respectively an attractive and a repulsive diabatic potential energy surface, or it could simply be a centrifugal barrier (see second term in Eq. (10)). Recently Museth *et al.* [1] also found evidence of a shape resonance in a model system of two purely repulsive diabatic surfaces, see Fig. 2. For energies above the threshold of the barrier and near eigenenergies of the "binding" part of the Hamiltonian (e.g. the zero-order Hamiltonian in the absence of non-adiabatic coupling), the system forms standing waves in the well and leaks out through the barrier via a tunneling mechanism. Thus shape resonances can occur in a simple one dimensional system.

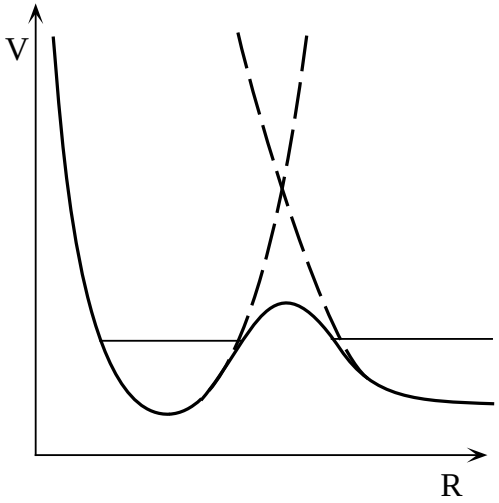

FIG. 1. Shape resonances correspond to standing waves of the system that tunnel out through a barrier. The barrier is the result of an non-adiabatic coupling between the two diabatic surfaces (the dashed curves)

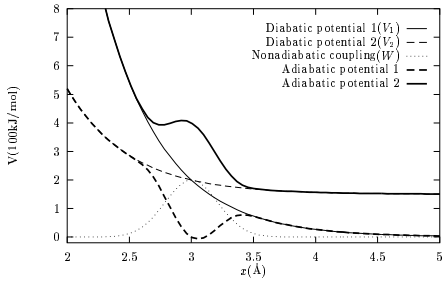

FIG. 2. Museth *et al.* [1] recently found this model system of two purely repulsive diabatic surfaces to support a shape resonance at 400 kJ/mol. The resonanse is formed in the small well on the upper adiabatic potential.

Feshbach or inelastic resonances, on the other hand, are associated with energy transfer from translational motion to some internal degree of freedom. In Fig. 3, a continuum state is coupled to some bound state of the vibrational motion, and by this redistribution of the collision energy the system is trapped. Energy then flows back from the vibrational to the translational mode, and eventually enough energy is accumulated in the dissociative coordinate to enable the system to escape.

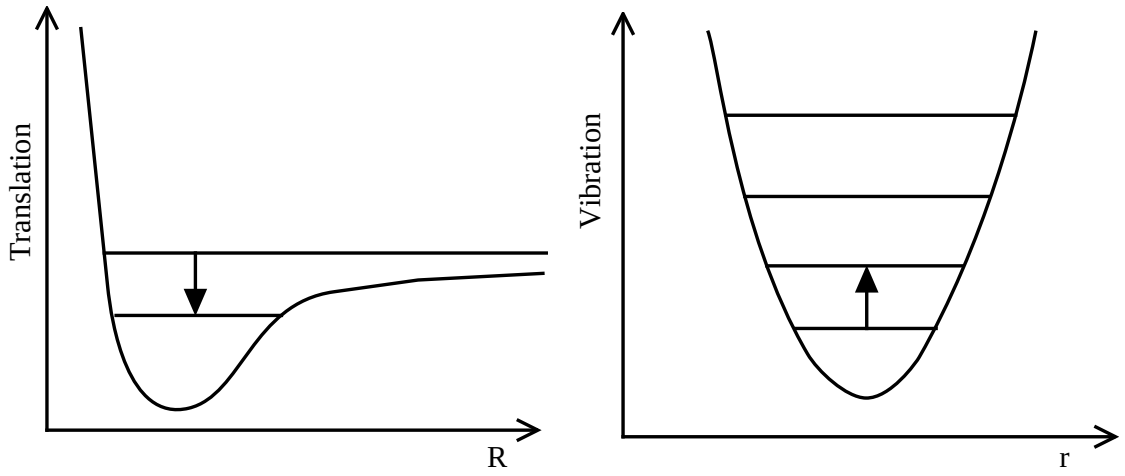

FIG. 3. When continuum states in the translational motion couple to bound states of some internal degree of motion (e.g. vibration) Feshbach resonances are formed.

The existence of such resonance states in many molecular reactions show up as complicated structures in the cross sections (cf. Fig. 1 in Ref. [1] and Fig. 3 in Ref. [2]) and thus constitutes an important physical phenomenon that must be taken into account when rationalizing anomalous behaviors in scattering data. However, the amount of work associated with the locations of the energy positions and life-times of the resonances have been a serious problem to theoreticians for many years. One way to efficiently characterize such resonances is through the use of so-called complex methods, as will be discussed later on.

The objective of this paper is twofold: First we want to re-examine the resonances of the $H^+ + O_2$ system, employing a different method than the close coupling approach previously used by Grimbert *et al.* [2]. The method of choice is the so-called "optical potential method" (OPM). The second objective is to evaluate this method against the close coupling approach, hoping to be able to set up a computational scheme which is more general and effective in the sense that it enables us to calculate and subsequently isolate all the resonances in one step.

Thus this paper reviews the OPM, summarize some techniques and tools to isolate and verify the resonances and subsequently reports calculations of resonance energies and widths for the electronically elastic $H^+ + O_2$ collision described in the framework of the Infinite-Order Sudden (IOS) approximation. The positions are shown to be in reasonable agreement

with previous results obtained for the system using close coupling equations [2]. However, we also observe very long-lived resonances that were not reported before.

The paper is organized as follows. Sec. II gives a short introduction to the methodology used in the description of resonance states and briefly mentions some of the most important methods that have been used in the past to characterize resonances. Focus is especially given to the complex methods on which this work is based. This brief introduction is meant as a "conceptual tool box" for many of the discussions in the forthcoming sections. Sec. III presents the overall numerical scheme in which a negative imaginary potential is added to the asymptotic part of the electronic potential energy surface. In Sec. IV we present the numerical results obtained using this optical potential method and compare the resonance positions and widths with previous results for this system in the framework of the IOS approximation. Finally Sec. V concludes and sums up the most important features of the optical potential method.

II. CHARACTERIZING RESONANCES

In quantum mechanics we solve the Schrödinger equation subject to boundary conditions to ensure that certain physical requirements are met. In the case of a simple scattering problem we write the asymptotic form of the wave function as

$$\psi(kr) \xrightarrow[r\to\infty]{} e^{-ikr} - S(k)\, e^{ikr} \tag{1}$$

where $k^2 = 2\mu E/\hbar^2 > 0$ and the ratio between the incoming and outgoing components of the continuum wave function is given by the celebrated S-matrix, $S(k)$. When dealing with bound problems the physics require that the solution is square integrable, i.e. the solutions are in the Hermitian domain of the Hamiltonian, and the energy is real negative. Hence we can write the boundary condition as

$$\psi(kr) \xrightarrow[r\to\infty]{} e^{-\kappa r} \tag{2}$$

where $\kappa > 0$. Comparing this expression to the general boundary conditions listed in Eq. (1), it is easy to see that stationary states correspond to solutions to a scattering problem with a negative imaginary wave number, $k = -i\kappa$, at a node of the S-matrix, $S(k) = 0$. Resonances on the other hand, are on physical grounds defined as wave functions with pure outgoing (Siegert state [3]) boundary conditions

$$\psi(kr) \xrightarrow[r\to\infty]{} e^{ikr} = e^{i\kappa_0 r} e^{\kappa_1 r} \tag{3}$$

where $\kappa_0 > 0$ and $\kappa_1 > 0$, i.e. $k = \kappa_0 - i\kappa_1$. If we again compare this expression to Eq. (1), we see that resonance states have $S(-k) = 0$ for complex k. Noting the simple relation [4] $S(k) = S(-k)^{-1}$, we arrive at the well known characteristics that resonance states are associated with poles of the S-matrix for complex values of the energy. The explanation of this divergence property of the resonance wave function in Eq. (3), ($|\psi(r\to\infty)|^2 = e^{2\kappa_1 r}$) and a simple physical interpretation of the complex energy, emerge if we consider a stationary solution to the time-dependent Schrödinger equation. If $\psi(r)$ is a solution to

the time-independent Schrödinger equation, satisfying Eq. (3), the solution to the time-dependent problem reads as $\Psi(r,t) = \psi(r)\, exp(-i\epsilon t/\hbar)$, where the energy is a complex number $\epsilon = E - i\Gamma/2$. Consequently the probability density of the resonance state is not time-independent in contrast to a bound state, but rather it leaks in time as

$$\begin{aligned} |\Psi(r,t)|^2 &= |\psi(r)|^2 exp(-i\,(\epsilon - \epsilon^*))\, t/\hbar \\ &= |\psi(r)|^2 exp(-\Gamma t/\hbar) \end{aligned} \tag{4}$$

and $\Gamma = 2\kappa_0\kappa_1\hbar^2/\mu > 0$ can now be identified as the rate constant (or width) of the exponentially decaying state. Noting that the lifetime is $\tau = \hbar/\Gamma$, we conclude that the negative imaginary energy of a resonance is associated to the inverse lifetime, and the real part of the energy, $E = (\kappa_0{}^2 - \kappa_1{}^2)\,\hbar^2/(2\mu)$, is referred to as the position of the resonance. We also note that the divergent property of Eq. (3) is a consequence of the conservation law of the number of particles in coordinate and time space [5] ($|\Psi(r \to \infty, t \to \infty)|^2 = \text{Const.}$). Finally we point out yet another very interesting and important consequence of the definition of a resonance state. Let us first assume that we are investigating resonances in a narrow energy window (i.e. $\kappa_0^2 - \kappa_1^2 \propto E \approx \text{Const.}$). In this case the width will be a growing function of the negative imaginary part of the momentum (cf. $\Gamma \propto \kappa_1\sqrt{\text{Const.} + \kappa_1^2}$). It next follows directly from Eq. (3) that the more broad (i.e. short-lived) a resonance is, the more divergent is the asymptotic part of the wave function, when compared to other resonances with the approximate same energy position. We especially note that sharp (or long-lived) resonances have a very small asymptotic amplitude as compared to broad resonances (or continuum states) in the small energy domain of interest. This is an important feature of quasi-bound states that we will refer to many times in the preceding sections of the paper.

Actually, decaying states, as defined in Eq. (4), were already introduced into quantum mechanics in 1928 by Gamow [6], and hence they are some times referred to as Gamow states in the literature. At this point we would like to quote Landau [7]: "Although decaying states may appear as just an academic exercise, they are probably more realistic than conventional quantum mechanics; if we wait long enough many (if not all) particles, nuclei and atoms do

decay in time and thus must be described as a type of Gamow state."

Two important consequences follow immediately from the simple characterization of a resonance state given above. Since the energy must be real positive in any scattering experiment, one can never have a system which is only decaying. Hence resonances are always accompanied by, often numerous discretized, continuum states. Furthermore, from a "methodical" point of view, the complex value of the resonance energy and the divergent property of $\psi(r)$ mean that we can not obtain resonance states simply by solving the Hermitian Schrödinger equation subject to real boundary conditions. In other words the numerical methods developed for bound problems are not directly applicable to the treatment of resonance states. This is a complicating aspect in the theoretical study of resonances, and have lead to many different numerical methods.

One "brute force" way to locate resonances is of course to solve the coupled (vibrational) set of equations with the Siegert state asymptotic boundary conditions given in Eq. (3). Alternatively one can also solve the coupled equations subject to the general boundary conditions listed in Eq. (1), and then look for poles in the S-matrix [2] (i.e. rapid jumps of the resonance part of the phase shift through $\pi/2$ modulo π [7]). However both these direct approaches are very demanding in terms of computational time, as the calculation has to be repeated for many different collision energies. Especially if the system displays very sharp resonances (i.e. long-lived) one needs a very fine grid in the collision energy. Also the existence of short-lived resonances can give rise to problems when using these methods, since the exact position and width can be difficult to assign for very broad lines. Another method is the so-called stabilization method [8] where the system is placed in a box of slightly varying size. The resonance states are then found as the solutions to the L^2 problem that are stable with respect to small variations of the box-size. This is a very easy scheme to implement, but it inherits some of the problems associated to the more direct methods mentioned above. A way to overcome these problems more generally is to extend the quantum mechanics to non-Hermitian Hamiltonians, which lead us to what we shall refer to as the complex methods (CCM and OPM).

In the complex coordinate method [5] (CCM), the reaction coordinate (e.g. R) in the total Hamiltonian is complex scaled, and the resulting non-Hermitian eigenvalue problem is solved using standard complex eigenvalue routines. Formally one encloses the system in a box (L^2 method) and transforms the Hamiltonian, $\widehat{H}(R)$, according to

$$\widehat{H}(R) \rightarrow \widehat{H}\left(Re^{i\theta}\right) \equiv \widehat{H}^{\theta} \tag{5}$$

The resonances correspond [9–11] to the complex eigenvalues, ϵ_n, of $\widehat{H}^{\theta}$ which are stable with respect to variation of the parameter θ, i.e. $\partial\Re[\epsilon_n]/\partial\theta = \partial\Im[\epsilon_n]/\partial\theta = 0$. The computational advantage of this variational complex method is that it isolates, in principle, all the resonance states from the continuum states as stationary points in the complex energy plane of θ-trajectories. Also, as this is an L^2 method it enables us to use numerical techniques developed for bound state problems. The CCM has been applied successfully to many different physical systems [12–15], but it should be clear from Eq. (5), that the analytical complex continuation of the Hamiltonian can only be accomplished when one has an analytical expression for the potential energy function. In other words the CCM has for many years mainly been restricted to simple model systems. However by using the identity

$$\begin{aligned} H^{\theta}_{m,n} &\equiv \int_R dR \left\{\Phi_m(R)\,\widehat{H}\left(e^{i\theta}R\right)\Phi_n(R)\right\} \\ &= e^{-i\theta}\int_{Re^{i\theta}} dR \left\{\Phi_m\left(e^{-i\theta}R\right)\widehat{H}(R)\,\Phi_n\left(e^{-i\theta}R\right)\right\} \end{aligned} \tag{6}$$

the complex scaling is shifted from the Hamiltonian to the (real) basis functions, $\Phi_m(R)$, which are in turn known analytically. This method of "backward scaling" the basis functions as opposed to "forward scaling the Hamiltonian", was first applied by Moiseyev and Corcoran [16,17] and Museth *et al.* [18] have recently presented a numerical scheme where matrix elements expressed in a multi dimensional discrete variable representation (DVR) are backward scaled to give the equivalent of Eq. (6).

The other complex method, which was initially proposed by Jolicard and Austin [19], consist of adding a local optical potential (OP) in the asymptotic region of the potential energy function. This optical potential method (OPM) is an L^2 method where one of the

tasks of the OP is to prevent reflection and transmission from the artificial box boundaries. By varying the amplitude of the OP the system is slightly perturbed and resonances show up as stable eigenfunctions of the non-Hermitian Hamiltonian, i.e. $\partial\Re[\epsilon_n]/\partial\Lambda = \partial\Im[\epsilon_n]/\partial\Lambda = 0$, where Λ is the amplitude parameter in the OP. Naively one could say that this method resembles the stabilization method mentioned above where the system is perturbed at the boundary. However it is important to emphasize that the OPM is an extension of quantum mechanics to the non-Hermitian domain of the Hamiltonian much like the CCM. Actually Rom, Lipkin and Moiseyev [20] have shown that by a specific choice of the local optical potential (a complex potential) the CCM can be shown to be identical to an optical potential method. In practice, however, the optical potential is often chosen as a simple negative imaginary potential (NIP) know from time-dependent molecular dynamics [21–23]. Consequently, the OPM with an arbitrary optical potential may shift the actual position and width of the resonances. The CCM on the other hand is based on rigorous mathematics, and hence the complex scaling expressed in Eq. (5) or Eq. (6) is guaranteed to give the correct resonances (within the framework of a finite basis set). Another drawback of the OPM is that in principle the NIP should be perfectly absorbing in the whole energy range of interest, which is practically unattainable as the amplitude of the NIP is a variational parameter in this scheme. Hence boundary effects created by the finite nature of the basis set can be significant. However, when all this has been said about the OPM it should be stressed that this method has important advantages over the CCM. First, the overall numerical scheme is very simple, and we need not worry about the analytical nature of the potential energy term. Secondly, there exist good candidates in the literature for almost perfectly absorbing NIP's [24,25], and finally the OPM allows for a self-correcting scheme. Using the generalized Hellman-Feynman theorem, Jolicard and Humbert [26] have shown that for two successive calculations of the complex resonance energy, made for the two values Λ_1 and Λ_2 of the amplitude parameter in the NIP, a corrected energy is given by

$$\epsilon_{res} = \epsilon_{\Lambda_2} + \frac{\epsilon_{\Lambda_1} - \epsilon_{\Lambda_2}}{1 - \epsilon'_{\Lambda_1}/\epsilon'_{\Lambda_2}} \tag{7}$$

where $\epsilon'_\Lambda = \partial\epsilon/\partial\Lambda = \left\langle \Phi^\dagger_\Lambda \left| \partial V_{opt}/\partial\Lambda \right| \Phi_\Lambda \right\rangle$. The associated corrected resonance eigenfunction reads as

$$\Phi_{res} = \Phi_{\Lambda_2} + \frac{\Phi_{\Lambda_1} - \Phi_{\Lambda_2}}{1 - \epsilon'_{\Lambda_1}/\epsilon'_{\Lambda_2}} \tag{8}$$

The existence of such a self-correcting scheme combined with the overall ease of the numerical implementation of the OPM made us choose this method for the study of resonances in the electronically elastic $H^+ + O_2$ collision to be presented in this paper. However, as will be clarified in the conclusion, this is not to say that we expect this method to give the final conclusive results, and at this point we can not rule out the necessity of future studies using the exact CCM.

III. METHOD OF CALCULATION

In this section we present the overall numerical scheme for our implementation of the optical potential method outlined in Sec. II. The Infinite-Order Sudden approximation (IOS) and its limitations will not be explained in great detail, we instead refer to a review paper by Baer [27] and the references mentioned therein. The numerical scheme is formulated in terms of an optimized discrete variable representation (DVR) of the two dimensional wave function. Some of the details of the DVR-scheme have been moved to the appendix, but for more information on the DVR/FBR-scheme and other applications of it see Ref. [28,18,29].

An important objective of the work presented in this paper is to reproduce the positions and widths of the resonances in the $H^+ + O_2$ system calculated by Grimbert *et al.* [2]. Thus we are going to make the same approximations for the collision, i.e. the study is carried out in the framework of the IOS approximation [27] where the relative angle γ is fixed to 45^o, cf. Fig. 4. Ion-molecule systems usually differ significantly from atom-molecule systems because the potential is more attractive and less dependent on the orientation angle γ [30,31]. Grimbert *et al.* [2] further argue that since the lifetimes of the resonances in $H^+ + O_2$, with the exception of two, are found to be small compared to the characteristic rotation time of an O_2 molecule (of the order of 10^{-11} s), the IOS approximation is justifiable. Thus except if mentioned otherwise, the parametrical γ dependence is omitted throughout the rest of this section.

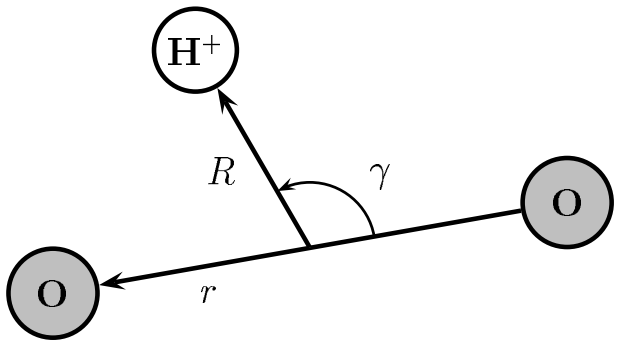

FIG. 4. Definition of the translational coordinates R, the vibrational coordinate r and the fixed relative angle γ.

A. The IOS Hamiltonian

In the IOS approximation the Hamiltonian for the system under consideration reads as

$$\widehat{H}(r,R) = -\frac{\hbar^2}{2\mu_{tot}}\frac{\partial^2}{\partial R^2} - \frac{\hbar^2}{2\mu_{O_2}}\frac{\partial^2}{\partial r^2} + \frac{\hbar^2\ell(\ell+1)}{2\mu_{tot}R^2} + V(r,R) \tag{9}$$

$$\equiv \widehat{T}_R + \frac{\hbar^2\ell(\ell+1)}{2\mu_{tot}R^2} + \widehat{h}(r,R) \tag{10}$$

where ℓ is the relative orbital angular momentum and $\widehat{h}(r,R) \equiv \widehat{T}_r + V(r,R)$ is an O_2 Hamiltonian depending parametrically on R. The definition of the two Jacobi coordinates r and R is illustrated in Fig. 4. We further define the zero order translational Hamiltonian

$$\widehat{H}_0(R) \equiv \widehat{T}_R + \frac{\hbar^2\ell(\ell+1)}{2\mu_{tot}R^2} + V_{eff}(R) \tag{11}$$

where the effective potential, $V_{eff}(R)$, is defined as the minimum of $V(r,R)$ with respect to the vibrational coordinate r. In the next two subsections we will define a complete basis set in r and R, which shall serve as the working basis set when we later set up the non-Hermitian Hamiltonian, and subsequently diagonalize it. To obtain an optimized basis set we will use a scheme with "preconditioning in the zero-order Hamiltonians" defined above, and subsequently truncate the basis set according to some *fictive* total translational energy (E_{tot}), so that we end up with a compact basis set. However, it is very important to emphasize that this collision energy does not explicitly enter the overall scheme for the optical potential method - only when we design the basis set. This is exactly one of the advantages of the complex methods as mentioned in the previous section. Thus, when E_{tot} is mentioned in the preceding subsections it should be interpreted as some sort of truncation parameter rather than an actual total translational energy.

B. Definition of FBR and DVR in the translational coordinate

In the translational coordinate R, we use a primitive FBR basis set of particle-in-a-box (PIB) sin-functions. These basis functions are simple periodical L^2 functions that define a DVR basis set in a very simple way, see the appendix. We start by defining the box

for the translational coordinate. As this coordinate is clearly not "bounded" we will have to provide the box parameters R_{min} and R_{max} by some means of guessing, based on the topology of the potential energy surface, $V_{eff}(R)$ in Eq. (11), and subsequently test for convergence. It should be noted that the presence of long-range multipolar interactions in ion-molecule systems, like $H^+ + O_2$, results in a much larger value of R_{max} than for the corresponding neutral atom-molecule system. Next we shift the domain of R to go from zero to $R_{max} - R_{min}$ and define the size of the FBR and the associated DVR basis set, by specifying the underlying grid. As mentioned in the appendix, the PIB-DVR has an equidistant or uniform grid, and a simple classical analysis of the de Broglie wavelength gives a grid spacing of

$$\Delta R = \frac{\lambda_{min}}{2\eta} = \frac{\pi\hbar}{\eta\sqrt{2\left(E_{tot} - V_{min}\right)\mu_{tot}}} \tag{12}$$

where η is a parameter larger than unity. The primitive normalized FBR basis set is thus defined as

$$\left\{\varphi_n(R) \equiv \sqrt{\frac{2}{R_{max}}}\sin\left(\frac{n\pi R}{R_{max}}\right), \quad n = 1, 2, \ldots, N_R \quad , R \in [0; R_{max} - R_{min}]\right\} \tag{13}$$

where $N_R = (R_{max} - R_{min})/\Delta R - 1$, and as discussed in the appendix, it is isomorphic to a DVR basis set, $\{|\mathcal{R}_p\rangle,\ p = 1, N_R\}$, cf. Eq. (A2). This DVR and the underlying uniform grid, $\{R_p,\ p = 1, N_R\}$, will constitute the "lowest-level" basis set in the R coordinate, and we shall not give any further reference to the explicit FBR in Eq. (13). It should be clear from the context that so far the working basis set has not been optimized for the numerical problem at hand – or to use a DVR terminology – the grid points have not been chosen as to reflect the physics of the problem. In other words we would like to have a DVR grid that reflects the topology of the potential energy surface such that the grid is dense in regions where the de Broglie wavelength (cf. Eq. (12)) is small and more sparse elsewhere. To obtain this we employ an optimizing scheme [32,33,18] based on the work of Harris, Engerholm and Gwinn (HEG) [34]. Using the basic property of the PIB-DVR (see Eq. (A4) and Eq. (A5))

we first construct a set of eigenfunctions of the zero-order Hamiltonian defined in Eq. (11)

$$\widehat{H}_0|q\rangle = E_q^0|q\rangle, \quad |q\rangle = \sum_{p\,=\,1}^{N_R} \langle \mathcal{R}_p|q\rangle|\mathcal{R}_p\rangle \tag{14}$$

This basis set, $\{|q\rangle,\ q = 1, N_R\}$, is then truncated according to a given collision energy E_{tot}. The resulting compact basis set, $\left\{|q\rangle,\ q = 1, N_R^{HEG} < N_R\right\}$, is then used to construct a new DVR basis set by diagonalizing the position operator

$$\widehat{R}|\mathcal{R}_q\rangle = R_q|\mathcal{R}_q\rangle, \quad |\mathcal{R}_q\rangle = \sum_{p\,=\,1}^{N_R} \langle \mathcal{R}_p|\mathcal{R}_q\rangle|\mathcal{R}_p\rangle \tag{15}$$

This set of eigenvalue equations thus defines a compact DVR basis set, $\left\{|\mathcal{R}_q\rangle,\ q = 1, N_R^{HEG}\right\}$, with the optimized grid points given as the eigenvalues. Note that the new HEG grid, $\left\{R_q,\ q = 1, N_R^{HEG}\right\}$, as opposed to the original PIB grid, $\{R_p,\ p = 1, N_R\}$, is not uniform. This optimized HEG-DVR basis set will constitute the working basis set in the coordinate R. As it is a DVR, the potential energy function is simply diagonal in this basis (Eq. (A4)), and the kinetic energy term is easily constructed by transforming back to the PIB-DVR (Eq. (15)) and then using the analytical expression of the FBR (Eq. (A5) or Eq. (A6)).

C. Definition of FBR and DVR in the vibrational coordinate

For the vibrational coordinate r we also use a primitive FBR basis set of PIB sin-functions. Hence we proceed in an analogous way to the previous section, except in this case the size of the r-box is determined from the fact that the system is bound in this degree of freedom. Thus r_{min} and r_{max} are given as the classical turning points for the potential energy surface at the energy E_{tot}. Consequently Eq. (12), Eq. (13) and the appendix also apply for the vibrational coordinate when the substitution $R \rightarrow r$ has been made, but it is important to emphasize that the constructed FBR/DVR scheme is of much smaller dimensionality than for the unbound R coordinate (i.e. $N_r < N_R^{HEG} < N_R$). In the PIB-DVR for r, we next setup a set of eigenvalue equations for the fixed R Hamiltonian, $\widehat{h}\,(R_q)$, defined in Eq. (10).

$$\widehat{h}\,(R_q)\,|m, q\rangle = E_m\,(R_q)\,|m, q\rangle \tag{16}$$

This defines a set of *adiabatic* vibrational states in each of the HEG grid points obtained through Eq. (15). At each individual grid point, R_q, the constructed adiabatic basis set, $\{|m,q\rangle,\ m=1,N_r\}$, is then truncated at $E_{tot} \approx E_v\left(R_{N_R^{HEG}}\right)$ corresponding to the energy in the lowest vibrationally *closed* channel $H^+ + O_2(v)$. That is, for each HEG grid point, R_q, we define a truncation parameter N_r^q such that

$$E_{N_r^q}(R_q) \ \leq \ E_v\left(R_{N_R^{HEG}}\right) \approx E_{tot} < E_{N_r^q+1}(R_q) \tag{17}$$

We can then contract this compact adiabatic basis into a new complete direct product basis set with the HEG-DVR defined in Eq. (15). Thus we finally define the working basis set as

$$\left\{|m,\mathcal{R}_q\rangle, \quad m=1,2,\ldots,N_r^q; \quad q=1,2,\ldots,N_R^{HEG}\right\} \tag{18}$$

where $|m,\mathcal{R}_q\rangle \equiv |m,q\rangle|\mathcal{R}_q\rangle$ is a basis function of both coordinates r and R.

D. Addition of the optical potential

As mentioned in Sec. II the OPM is essentially a non-Hermitian variational method in the amplitude parameter of a NIP added to the asymptotic part of the potential energy function. Many different kinds of NIPs have been proposed in the literature [21–24], and we choose an exponential form whose absorbing properties have been investigated thoroughly by Vibók and Balint-Kurti [25]. Thus the NIP, $V_{opt}(R)$, read as

$$V_{opt}\,(R) = \begin{cases} 0 & \text{for} \quad R_{min} \leq R \leq R_0 \\ -i\Lambda N \exp\ \left(-2\frac{R_{max}-R_0}{R-R_0}\right) & \text{for} \quad R_0 < R \leq R_{max} \end{cases} \tag{19}$$

where Λ is a premultiplier used to minimize the reflection and transmission from the potential and N is a normalization constant found numerically to be 13.22 [25]. For a given energy domain Vibók *et al.* [25] provide optimized tabulated values for the parameter Λ and the range of definition, $\Delta R_{opt} \equiv R_{max} - R_{min}$. However in the present application of the optical potential to locate resonances, the premultiplier Λ is not a fixed parameter, but rather a

variational amplitude parameter. Thus, we cannot simply followed the guidelines given in Ref. [25] to assign $\{\Lambda, \Delta R_{opt}\}$. Instead we have to used many different values of ΔR_{opt} to test for convergence. This clearly emphasizes yet another drawback of the OPM, as compared to the CCM; the added optical potential introduces new parameters into the numerical scheme. This usually means a lot of additional convergence tests to determine these parameters.

The optical potential, Eq. (19), is added to the total Hamiltonian, Eq. (9), and for different values of the parameter Λ a matrix representation of this non-Hermitian Hamiltonian is then computed in the basis set derived above, Eq. (18). It is important to note that since the optical potential is only a function of R, and the complete basis set is a DVR in this coordinate, the addition of the NIP just adds complex values of V_{opt} (at the HEG grid points) to the diagonal. Thus the DVR in the translational coordinate, makes the implementation of the optical potential method very easy. The computed complex symmetric matrix is next diagonalized for many different values of Λ, and for successive calculations in Λ the produced complex eigenvalues are connected using a maximum-overlap scheme for the associated complex eigenvectors. Finally the Λ-trajectories are plotted in the complex energy plane with the real part (i.e. energy position) along the positive x-axis and the imaginary part (i.e. half width) along the negative y-axis. A visual inspection of each trajectory next follow in order to determine which ones correspond to ether a bound, continuum or resonance state. The bound states are not affected by the presence of the NIP placed in the asymptotic region, and hence they show up as coinciding dots on the real energy axis *below* the value of the threshold energy, i.e. the zero-order vibrational energy in the entrance channel. (Bound states have in principle an infinitely large lifetime corresponding to zero width, i.e. no imaginary energy component). The resonance and continuum states, on the other hand, are only found *above* this value of the threshold energy. The later have amplitude in the whole coordinate space and hence they are very sensitive to small changes in the NIP. Consequently the continuum states correspond to trajectories which are continuously rotated into the negative imaginary energy plane as the amplitude parameter, Λ, increases. From the theory of resonances by complex methods it follows that resonance, or quasi-bound states,

are visually identified as stagnation points or cusps in the complex energy plane. However, it is very important to emphasize that these simple characteristics of the three different types of states are not generally sufficient as a guideline to isolate resonance states when using the optical potential method. The reason for this complicating aspect of the optical potential method is of course that this is an approximate method as pointed out in Sec. II. The presence of the NIP slightly perturbs the system in a non-physical way, thereby casing it to change its characteristic behavior under the complex scaling, i.e. variation of Λ. This means that some times continuum trajectories can behave as resonance trajectories and vice versa. Especially for large values of Λ, i.e. for large perturbations from the NIP, can one observe spurious behaviors of the complex trajectories. All in all this means that one has to be a little careful before a final identification of a resonance state can be made. In other words we need additional techniques or tools to verify the existence of a resonance after it has been isolated. We have come up with the following simple tests

1. Perform a convergence test by slightly chancing the remaining parameters entering the definition of the negative imaginary potential. We found it to be especially useful to repeat the calculations with different values of the domain of definition for the NIP. Trajectories corresponding to a real physical resonance will show very little effect on these changes in the domain of Λ where the quasi-bound states are formed. "Ghost-trajectories", on the other hand, will not show the same invariance with respect to these variations, and often one observes dramatic changes of the trajectory for all values of Λ. (See Fig. 6 and Fig. 7 in the next section for an illustration).

2. Alternatively one can graphically plot the amplitude of the state vector calculated at the value of Λ where the stagnation point is observed. As pointed out in Sec. II the divergent property of the asymptotic part of a resonance wave function increases with the width (assuming $E \approx$ Const.). Resonances will show a large amplitude in the interaction region (with vibrational excitation for Feshbach resonances) and a relatively small periodic amplitude in the entrance channel corresponding to the pure outgoing

boundary condition mentioned in Sec. II Eq. (3). Continuum states (i.e. . $\Gamma \to \infty$) on the other hand will display a relatively large amplitude in the asymptotic regions of the channel. For very sharp resonances it can actually be difficult the distinguish a resonance state from a bound state since it has almost negligible amplitude at the boundary. Thus, if one first filters off all the bound states by truncating the trajectories below the threshold energy this test is very useful - although a bit time consuming. This technique can of course also be used when applying the complex coordinate method [18], although this is in principle an exact method, and should therefore not give rise to spurious behavior of the trajectories. (See Fig. 8 and Fig. 9 in the next section for an illustration).

Finally we comment on the the self-correcting scheme by Jolicard, Eq. (7), as a tool to decide whether or not a trajectory corresponds to a resonance. We have not included this scheme in the list above for the following reason: We found that Eq. (7) only produces meaningful corrections to the resonance positions when the successive values of the variational parameters Λ_i are close to a resonance. Outside this domain of Λ, and for non-resonant states, Eq. (7) gives arbitrary complex values, which makes the visual tracking of the new chaotic Λ-trajectories in the complex energy plane extremely difficult. Thus in order to use this self-correcting scheme efficiently, the computer implementation should be able to separate the resonance trajectories from the continuum trajectories, and further choose the correct domain of Λ values for each resonance trajectories. However, as this is exactly the problem that we hoped to address by employing this scheme, we did not find it useful as a tool to verify a resonance, but rather to check for convergence when the verification was made by ether (1) or (2).

IV. NUMERICAL RESULTS

In all the reported calculations we have used the same collision conditions as Grimbert *et al.* [2], in order to compare with their results. Thus, a single value of the relative angle, $\gamma = 45°$ in Fig. 4, and an orbital angular momentum value, $\ell = 0$ in Eq. (9), are considered. The later implies that the barrier produced from the centrifugal term in Eq. (9) can be neglected, and consequently the system will only display *Feshbach* resonances under these circumstances. Further the collision energy is restricted to $E_{tot} < 0.2\,\mathrm{eV}$ as measured from the $H^+ + O_2$ $v = 0$ dissociation threshold. As in Ref. [2] we are also going to disregard the charge transfer channel, $H + O_2^+ \left(X^2\Pi_g\right)$, which leave us with an electronically elastic collision problem. All in all this implies that only the $v = 0$ channel is open (vibrational elastic scattering), such that $E_{v=1}$ in Eq. (17). Thus the calculated Feshbach resonances are of the type

$$\left[HO_2^+\right]^* \;\rightarrow\; H^+ \;+\; O_2\left(X^3\Sigma_g^-, v=0\right) \tag{20}$$

The diabatic electronic potential energy surface correlating with $H^+ + O_2\left(X^3\Sigma_g^-\right)$ is that of Grimbert *et al.* [35]. Numerical values of the corresponding potential on the HEG and PIB grid, defined in Sec. III, are obtained by a two dimensional spline interpolation in r and R, see Fig. 5. The box parameters in the two Jacobi coordinates are fixed to

$$\begin{aligned} R_{min} &= 0\,\mathrm{au} \qquad R_{max} = 20\,\mathrm{au} \\ r_{min} &= 1.5\,\mathrm{au} \qquad r_{max} = 2.9\,\mathrm{au} \end{aligned} \tag{21}$$

Since no data points are available in the interval going from $R = 15\,\mathrm{au}$ to $R = 30\,\mathrm{au}$ we used the value of the potential at $R = 30\,\mathrm{au}$ in this interval. This produces a slight discontinuity at $R = 15\,\mathrm{au}$ of the order of $0.02\,\mathrm{mHartree}$. However, this approximation is made in order to reserve some additional space for the domain of definition of the NIP. Perhaps a somewhat more disturbing feature is the cut-off of the surface of Ref. [35] at $r_{max} = 2.9\,\mathrm{au}$, see Fig. 5. At this value of the vibrational coordinate (and $R \approx 2 - 3\,\mathrm{au}$) the potential energy is far below the maximal collision energy of $0.2\,\mathrm{eV} \approx 7.3\,\mathrm{mHartree}$.

Consequently the potential energy surface we use in the calculations has an infinite wall at $r = 2.9\,\text{au}$. In the closed coupled calculations by Grimbert *et al.* [2] this caused no problems since they used vibrational eigenstates of $O_2\left(X^3\Sigma_g^-\right)$ as the basis-set in the r coordinate. Thus they employed a vibronic *diabatic* basis-set which has negligible amplitude at $r_{max} = 2.9\,\text{au}$. However, as explained in Sec. III C Eq. (16) we employ a vibronic *adiabatic* basis-set in r, which depend parametrically on the HEG grid points defined in Sec. III B. As mentioned before this makes it possible to construct a very optimized and compact basis-set, cf. Eq. (18), which so to speak follows the dynamics as the collision takes place. The problem, however, is that this adiabatic basis-set does not have the "built-in" boundary conditions that makes it ignore the presents of the infinite wall at large values of r. This is probably the most significant difference in the "physical setup" of the two calculations.

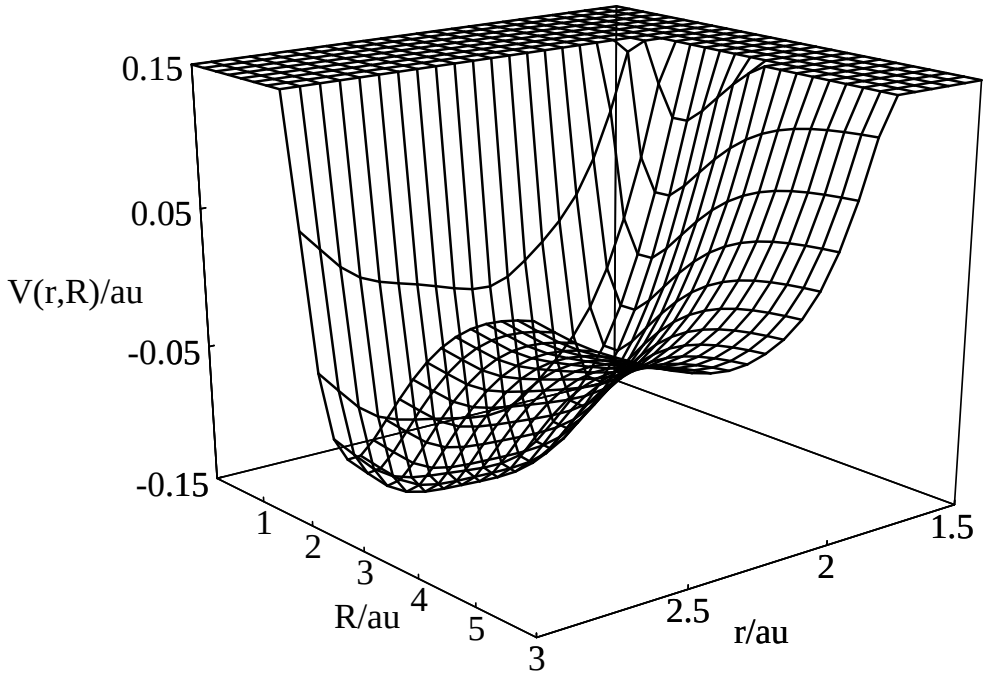

FIG. 5. Plot of the spline interpolated electronically diabatic potential energy surface correlating with $H^+ + O_2\left(X^3\Sigma_g^-\right)$ [35]. The definition of the two Jacobi coordinates r and R are illustrated in Fig. 4 and the relative angle γ is fixed at 45°. The origin of energies is the vibronic zero-point channel energy. (Note also the cut-off of the surface for large values of r).

Using the numerical method explained in Sec. III and the "physical setup" mentioned above we next performed calculations of resonances in the electronically elastic $H^+ + O_2$ collision. In these calculations we used 40 particle-in-a-box functions in r, and 350 in R. Using the HEG scheme the later basis set was truncated to 100 DVR functions. The truncation of the adiabatic states in r (Eq. (17)) gave 2 to 19 basis functions depending on R. Thus $N_r = 40$, $N_r^q = 2 - 19$, $N_R = 350$, and $N_R^{HEG} = 100$ in Sec. III, and the dimension of the contracted direct product basis, defined in Eq. (18), was in the order of 550. This was sufficient to obtain convergence for almost all of the resonances. The convergence was tested by employing the first of the techniques discussed in Sec. III D. Thus, we performed successive calculations with 5 different values for the domain of definition for the NIP. R_{max} in Eq. (19) was fixed as listed in Eq. (21) and R_0 was successively given values corresponding to $\Delta R_{opt} \equiv R_{max} - R_0 = 3, 4, 5, 6$ and 7 au. For each calculation, corresponding to a fixed ΔR_{opt}, the variational Λ parameter in Eq. (19) was changed from zero to 8×10^{-3} in 40 steps of 0.2×10^{-3}. This turned out to be sufficient to isolate all the resonances. In Fig. 6 and Fig. 7 we have plotted Λ-trajectories with different values of ΔR_{opt} corresponding to two characteristic situations. The trajectories are plotted in the complex energy plane with the real part (i.e. energy position) along the positive x-axis and the imaginary part (i.e. half width) along the negative y-axis. Fig. 6 shows an example of a typical continuum state which is very sensitive to small changes in the NIP. Note the spurious behavior of the trajectories with small values of ΔR_{opt}. They actually behave as a resonance state in the sense that they have stagnation points - although at different positions in the complex energy plane. However, this is not a "true resonance state", but rather a continuum state which is perturbed by an imperfect NIP. This is clearly seen from the trajectories obtained from calculations with a more perfect NIP (i.e. $\Delta R_{opt} > 5$ au) where the trajectories are continuously rotated into the negative imaginary energy plane as the amplitude parameter, Λ, increases. Thus, Fig. 6 clearly illustrates the need and importance of additional convergence/verification tests as discussed in Sec. III D; with only one calculation (e.g. $\Delta R_{opt} = 3$ au) one could erroneously confuse the continuum state in

Fig. 6 with a "true resonance state" as shown in Fig. 7. In the later situation (Fig. 7) the trajectories show very small changes with variations of ΔR_{opt} which is exactly what characterizes a resonance state. A close-up of the trajectories actually shows that for Λ and ΔR_{opt} large enough the calculated complex data points almost coincide. Thus, the true resonances state is only formed for specific values of *both* Λ and ΔR_{opt}. All the 5 trajectories in Fig. 7 show the characteristic behavior of a resonance state (i.e. a stagnation point), but only 3 of them actually correspond to a "true resonance". Again this emphasizes the importance of a convergence test; with only one calculation (e.g. $R_{opt} = 4\,\mathrm{au}$) one would obtain incorrect values of the resonance position and width. The variation of R_{opt} corresponds to changing the energy domain in which the NIP is an almost perfect absorber.

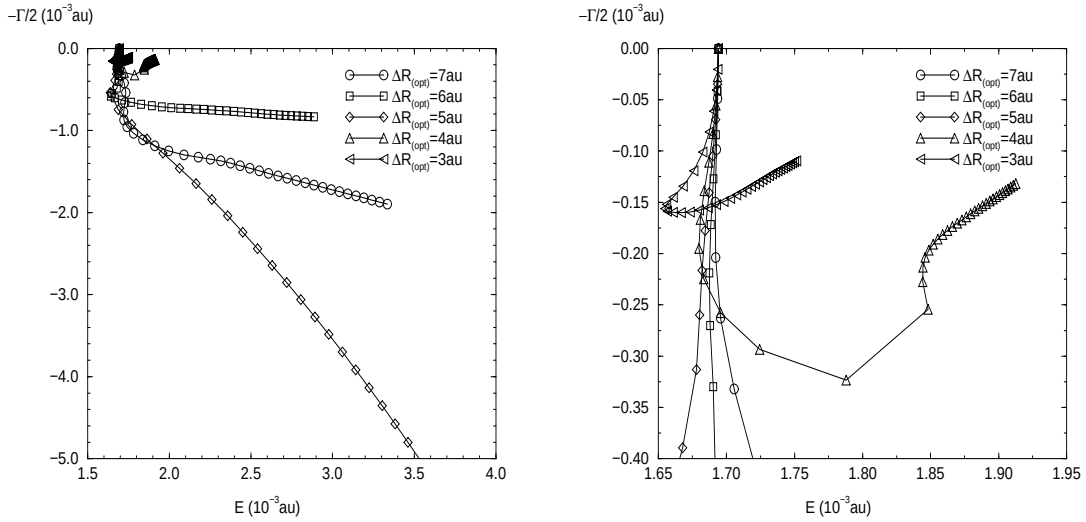

FIG. 6. Plots of complex energy trajectories for a continuum state, obtained from calculations with 5 different values of $\Delta R_{opt} \equiv R_{max} - R_0$ in Eq. (19). Each of the 5 trajectories are made up by 40 connected points corresponding to the different values of the variational Λ parameter entering Eq. (19). For almost all values of Λ the trajectories are clearly very sensitive to the changes in the optical potential. Note the *different* stagnation points for the $R_{opt} = 3$ and 4 au trajectories in the right close-up plot. See also Fig. 8 for a 3D-plot of the amplitude of this continuum state.

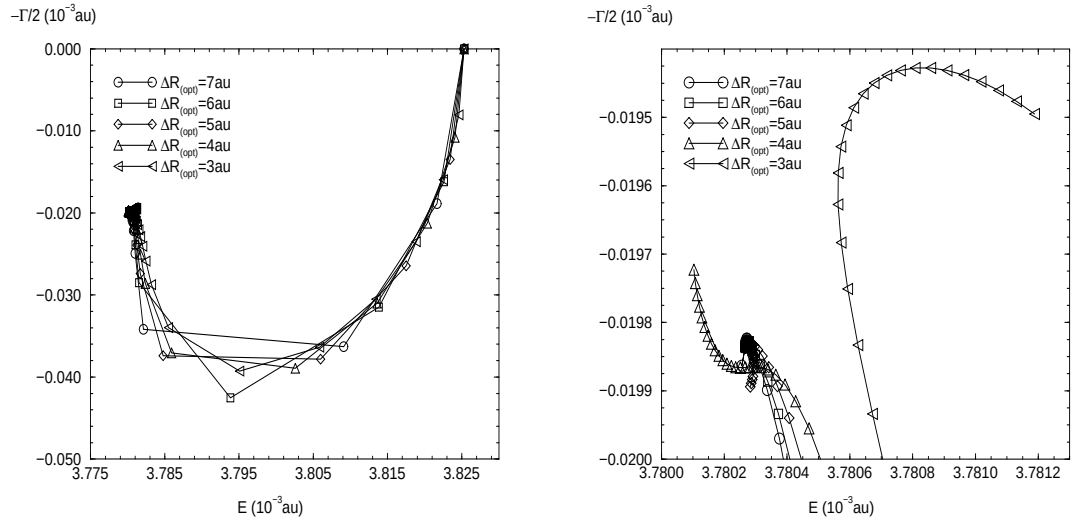

FIG. 7. Plots of complex energy trajectories for resonance state number 10 in Table I and Table II, obtained from calculations with 5 different values of $\Delta R_{opt} \equiv R_{max} - R_0$ in Eq. (19). Each of the 5 trajectories are made up by 40 connected points corresponding to the different values of the variational Λ parameter entering Eq. (19). For the last 20-30 values of Λ the trajectories are clearly very insensitive to the changes in the optical potential. Note the slight drifting of the stagnation points for the $R_{opt} = 3$ and 4 au trajectories in the right close-up plot caused by the imperfect NIP. See also Fig. 9 for a 3D-plot of the amplitude of this resonance state.

Finally we have shown a 3-dimensional plot of the wave function for the two characteristic situations illustrated in Fig. 6 and Fig. 7. Fig. 8 shows the divergent property of the continuum state in the asymptotic region of the configuration space (cf. Eq. (3) with large κ_1). As we do not impose any boundary conditions on the wave function (corresponding to the incoming part in Eq. (1)) continuum states show up as extremely broad resonances in the OPM formulation. The large amplitude in the entrance channel explains for the dramatic changes observed in Fig. 6 as the NIP (i.e. perturbation) is varied. Fig. 9 shows the resonance state with its characteristic shapes; large rapidly changing amplitude in the r-direction of the interaction region, corresponding to the vibrational excitation of a Feshbach resonance, and the small R-periodic amplitude in the asymptotic region of the channel which correspond to the purely outgoing boundary condition of a resonance (cf. Eq. (3)) as discussed in Sec. II.

Thus both of the techniques mentioned in Sec. III D were used to verify the resonances and subsequently check for convergence.

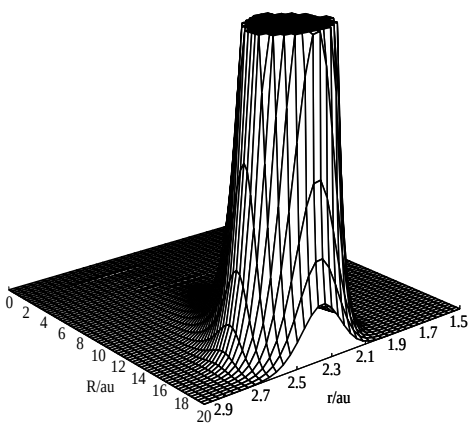

FIG. 8. Plot of the norm square of the amplitude for the continuum state shown in Fig. 6. In this calculation ΔR_{opt} and Λ, entering Eq. (19), were fixed at respectively 7 au and 4×10^{-3}, corresponding to the $20'th$ point on the $\Delta R_{opt} = 7$ au trajectory in Fig. 6. Note the divergent property of the continuum wave function in the asymptotic region of the configuration space.

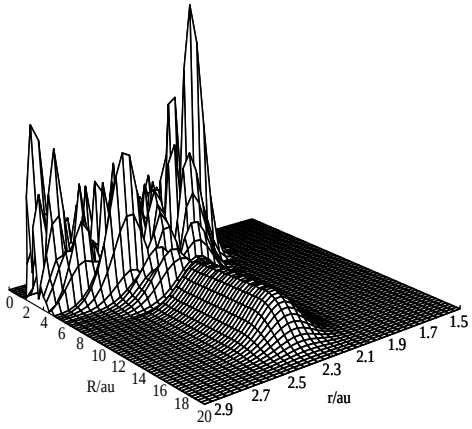

FIG. 9. Plot of the norm square of the amplitude for the resonance state shown in Fig. 7, and listed in Table I and Table II as number 10. In this calculation ΔR_{opt} and Λ, entering Eq. (19), were fixed at respectively 7 au and 4×10^{-3}, corresponding to the $20'th$ point on the $\Delta R_{opt} = 7$ au trajectory in Fig. 7. Note that the characteristic resonance wave function has large amplitude in the interaction region of the coordinate space and a very small amplitude in the entrance channel.

In Table I we have listed the calculated energy positions and associated widths for resonances below a collision energy of 7.3×10^{-3} Hartree, which is the energy domain investigated by Grimbert *et al.* [2]. The table reports the results form 5 different calculations corresponding to $\Delta R_{opt} = 3, 4, 5, 6$ and 7 au. It should be evident from this table that all the listed states are indeed resonances and not just "ghost-states", i.e. perturbated continuum states that merely behave as quasi-bound states (cf. Fig. 6). Actually, with the exception of res-

onance number 1,2,3,5,7,9,11,21 and 25, they all show complete invariance with respect to the changes in the NIP. However, of the sensitive resonances, some of them (cf. 3,5,7,9 and 11) even loose the characteristic stagnation point as ΔR_{opt} decreases, and thus start behaving as continuum states. A closer inspection of Table I furthermore shows that these sensitive states are all broad (i.e. short-lived) resonances. The reason for this behavior is easily explained when we recall the very definition and characteristic of a resonance state discussed in the introduction of Sec. II (cf. paragraphs below Eq. (3) and Eq. (4)). The amplitude in the asymptotic region of the entrance channel increase rapidly with the width of the resonance, and consequently the range needed to absorb the wave functions associated with narrow resonances is much less than for the broad ones. This is clearly reflected in Table I. However, increasing ΔR_{opt} eventually also means extending the R-box which can be very costly in terms of CPU-time. Also, the NIP is in practice only perfect in a very narrow energy-window, i.e. the NIP is almost always accompanied by some reflections from the boundary. This generally leads to shifting of the true energy positions and widths, but we expect these perturbations from the NIP to be predominant for the broad resonances where the asymptotic amplitude is large. All in all we conclude that the optical potential method seems best suited to study sharp resonances.

Table II shows a comparison of the converted resonances listed in Table I and earlier results obtained by Grimbert *et al.* [2] solving the coupled equations. The table shows 25 resonances, 18 of which correspond to the resonances located by Grimbert *et al.* For the large majority of the resonances, the positions are in acceptable agreement (i.e. $|\Delta E| < 0.15 \times 10^{-3}$ Hartree) with the previous calculations, but the widths are some times off by a factor as much as 10. It is however reassuring to see that there is a clear match in the variations of the widths in the two columns, but the deviations do not seem to follow any particular pattern. It is difficult to give a clear cut explanation for the deviations, but one could probably argue that we did not reproduce the exact collision conditions under which the study by Grimbert *et al.* was conducted. Resonances are widely known to be extremely sensitive to the curvature of the potential energy surface, and the extension of the surface beyond 15 au

might have influenced the calculations. However, as mentioned before we believe that the most significant difference in the "physical setup" of the two calculations is related to the different basis-set approaches. In the optical potential calculations presented in this article we employed a vibronic *adiabatic* basis-set of the order of 500 whereas Grimbert *et al.* used 14 vibronic *diabatic* basis functions to solve the coupled equations. Apart from the obvious difference in the sizes of the employed basis-sets, which is definitely in favor of the OPM, it should also be stressed that the underlying physical description of the collision differs in the two cases. The diabatic basis-set deals with the somewhat disturbing cut-off of the surface at $r_{max} = 2.9\,\mathrm{au}$ (cf. Fig. 5) in an ad hoc way, whereas the adiabatic basis-set does not. Consequently the surface exhibits a wall in the presented calculations which is not present in the previous studies by Grimbert *et al.* This clearly makes the comparison difficult. Finally we note that disagreements between the two compared methods have been observed before in the literature; Monnerville *et al.* [36] exactly finds a disagreement for broad resonances in the one-dimensional study of predissociation of CO. They argue that this is primarily due to the fact that close coupling approaches are generally not capable of correctly reproduce very broad resonances. The shape of the found resonances are not Lorentzian (i.e. asymmetric) which can give significant error-bars when assigning the resonance position and width. We can go along with this argument, but finds it equally important to emphasis that the OPM also has problems in this limit as pointed out above.

Table II also shows 7 new resonances, 4 (cf. 4,6,8 and 12) of which being very long-lived (i.e. $\tau > 10^{-10}\,\mathrm{s}$). It is interesting to see that the only new relatively short-lived resonances (cf. 13,14 and 20) are located in the most dense parts of the spectra which is also where the largest deviations are found (e.g. 16). Thus it seems plausible that Grimbert *et al.* [2] overlooked or simply missed these resonances because they overlapped. The finding of the new very sharp resonances is not very surprising considering the fact that the close coupling approach, used by Grimbert *et al.*, exactly has a problem isolating very sharp resonances unless the energy grid is equally very dense.

V. CONCLUSION

All the resonances found by Grimbert *et al.* [2] are confirmed, although the widths of some resonances are off by a factor of 10. In the previous section we have discussed some important issues that should provide arguments to explain the disagreement between the two approaches. We especially drew attention to the different basis-sets employed in the two calculations and further pointed out that both methods show weaknesses in the limit of very broad resonances. Given these facts we find the agreement acceptable, but stress that it is difficult to make a final conclusive evaluation of the found resonances relative to the previous results. However, it is striking that we found 7 new resonances, 4 of which were very long-lived, $\tau > 10^{-11}$ s. First of all this clearly shows what we expected from the very beginning, namely that the method of close coupled equations is not well suited to isolate sharp resonances, unless of course the energy grid is made very dense at the cost of computational time. We also note that the existence of these very long-lived resonances could well signify that the use of the IOS approximation, on this system, might be called in question. Grimbert *et al.* [2] argue that since they found no resonances with lifetimes comparable to the characteristic rotation time of the O_2 molecule (of the order of $10^{-11}s$), the IOS approximation was justifiable. Given the discovery of the new resonances we question this justification, but at the same time we acknowledge that this is by no means a definitive proof of the invalidity of the IOS approximation applied to the $H^+ + O_2$ system - it merely invalidates the way it has been justified in Ref. [2].

The present study also gives an examination of the optical potential method as an alternative to the close-coupled approach. We believe the OPM to be more accurate and general in the sense that it in principle isolates all the resonances in the complex energy plane in one step, i.e. we do not have to scan the real energy axis. The subsequent visual inspection of the complex trajectories is however rather tedious. This inconvenience of the OPM was further intensified by the present discovery of spurious behavior of the trajectories. This forced us to introduce additional techniques to isolate and verify the existence of a resonance state; we

especially focused on the convergence tests where we made small variations in the domain of definition of the NIP, and the 3-dimensional plotting of the corresponding wave function. To "routinely" overcome these problems discovered with the isolation of the resonances in the complex energy plane, and further in order to give a conclusive evaluation of the found results we will have to employ the "exact" complex coordinate method [18] mentioned in Sec. II.

ACKNOWLEDGMENTS

We would like to thank Georges Jolicard for helpful discussions concerning the optical potential method. This work was partially supported by the E.U. Human Capital and Mobility Program through the "Structure and Reactivity of Molecular Ions" network under contract # CHRX-CT93-0150, and by a grant of computer time from the Institut du Développement et des Ressources en Informatique Scientifique (IDRIS).

APPENDIX A: PARTICLE IN A BOX DVR

Consider a one-dimensional quantum system, with coordinate R restricted to an arbitrary but fixed box. First we note that any physical box can always be shifted without loss of generality. Thus for a given box in the coordinate R - going from *zero* to R_{max} - we can define a FBR basis set of normalized particle-in-a-box (PIB) sin-functions, see Eq. (13). The N_R roots of $\varphi_{N_R+1}(R)$ in the interval $]\,0;\ R_{max}\,[$

$$R_p = \frac{R_{max}}{N_R+1} p \equiv \Delta R\, p, \qquad p = 1, 2, \ldots, N_R \tag{A1}$$

are exactly the abscissas for the DVR associated with this FBR, and the corresponding weights, ω_p, can easily be shown to be the constant ΔR. The transformation from the DVR, $\{|\mathcal{R}_p\rangle,\ p = 1, N_R\}$, to the FBR, reads as

$$|\mathcal{R}_p\rangle = \sum_{n\ =\ 1}^{N_R} U_{pn} |\varphi_n\rangle \tag{A2}$$

where the *unitary* matrix $\underline{\underline{U}}$, is given by

$$U_{pn} \equiv \langle \mathcal{R}_p | \varphi_n \rangle = \sqrt{\frac{2}{N_R+1}} \sin\ \left(\frac{n\pi R_p}{R_{max}}\right) \tag{A3}$$

It is important to note that the endpoints of the box (i.e. 0 and R_{max}) are excluded in the definition of the grid points, see figure 10. The reason for this is that every member of the FBR basis set is zero at these points, resulting in zero-columns in $\underline{\underline{U}}$. Thus the matrix expressing the basis set transformation would not be unitary i.e. the defined DVR and FBR are not isomorphic.

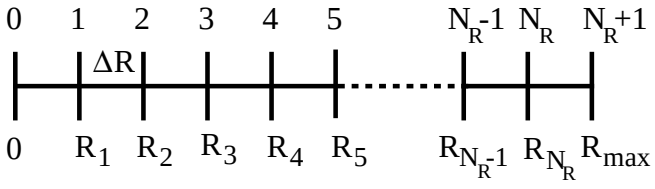

FIG. 10. Definition of the points in the uniform particle-in-a-box grid. Note that the endpoints are not included in the definition of the points.

Within the approximation of the associated quadrature the defined DVR satisfy the following basic relation

$$\langle \mathcal{R}_n \left| V\left(R\right) \right| R_{n'} \rangle = \delta_{nn'} V\left(R_n\right) \tag{A4}$$

and consequently the potential energy term in the Hamiltonian is simply diagonal in the DVR basis set. Using the analytical expression for the FBR (Eq. (13)) it is easy to show that the matrix representation of the kinetic energy operator in the DVR basis set reads as

$$\underline{\underline{T}} = -\frac{\hbar^2}{2\mu} \underline{\underline{U}} \cdot \underline{\underline{N}} \cdot \underline{\underline{U}}^{\dagger} \tag{A5}$$

where $N_{nn'} \equiv -(n\pi/R_{max})^2 \delta_{nn'}$ and $\underline{\underline{U}}$ is defined in eq A3. The evaluation of the matrix elements, T_{pq} in Eq. (A5), thus involve a sum over products of two sin-functions with the premultiplier n^2. After some tedious calculations (see footnote 20 in reference [29]) one can obtain the following analytical expression for the sum

$$T_{pq} = \frac{h^2(-1)^{p-q}}{4\mu R_{\mathbf{max}}^2} \times \begin{cases} F\left(p-q\right) - F\left(p+q\right) & \text{for } p \neq q \\ \left(2(N_R+1)^2+1\right)/3 - F\left(p+q\right) & \text{for } p = q \end{cases} \tag{A6}$$

where $F(n) \equiv \sin^{-2}\left(\frac{\pi n}{2(N_R+1)}\right)$.

[1] K. Museth and G. D. Billing, J. Chem. Phys. **105**, 9191 (1996).

[2] D. Grimbert, V. Sidis, and M. Sizun, Chem. Phys. Lett. **230**, 47 (1994).

[3] A. F. J. Siegert, Phys. Rep. **56**, 750 (1939).

[4] K. Smith, *The calculation of atomic collision processes*, John Wiley and Sons, University of Nabraska, 1971.

[5] N. Moiseyev, Isr. J. Chem. **31**, 311 (1991).

[6] G. Gamow, Z. Phys. **51**, 204 (1928).

[7] R. H. Landau, *Quantum Mechanics II*, John Wiley and Sons, New York, 1996.

[8] A. U. Hazi and H. S. Taylor, Phys. Rev. A **1**, 1109 (1970).

[9] E. Balslev and J. M. Combes, Commun. Math. Phys. **22**, 280 (1971).

[10] B. Simon, Commun. Math. Phys. **27**, 1 (1972).

[11] B. Simon, Math.Phys. **97**, 247 (1973).

[12] B. R. Junker, Adv. At. Mol. Phys. **18**, 207 (1982).

[13] W. P. Reinhardt, Annu. Rev. Phys. Chem. **33**, 223 (1983).

[14] N. Lipkin, N. Moiseyev, and J. Katriel, Chem. Phys. Lett. **147**, 603 (1988).

[15] N. Lipkin, N. Moiseyev, and C. Leforestier, J. Chem. Phys. **98**, 1888 (1993).

[16] N. Moiseyev and C. T. Corcoran, Phys. Rev. A **20**, 814 (1979).

[17] V. Ryaboy and N. Moiseyev, J. Chem. Phys. **103**, 4061 (1995).

[18] K. Museth and C. Leforestier, J. Chem. Phys. **104**, 7008 (1996).

[19] G. Jolicard and E. J. Austin, Chem. Phys. Lett. **21**, 106 (1985).

[20] N. Rom, N. Lipkin, and N. Moiseyev, Chem. Phys. **151**, 199 (1991).

[21] C. Leforestier and R. Wyatt, J. Phys. Chem. **78**, 2334 (1983).

[22] R. Kosloff and D. Kosloff, J.Comput.Phys. **63**, 363 (1986).

[23] D. Neuhauser and M. Baer, J. Chem. Phys. **90**, 4351 (1989).

[24] S. Brouard, D. Macias, and J. G. Muga, J. Phys. A **27**, L439 (1994).

[25] A. Vibók and G. Balint-Kurti, J. Phys. Chem. **96**, 8712 (1992).

[26] G. Jolicard and J. Humbert, Chem. Phys. **127**, 31 (1988).

[27] M. Baer, Adv. Chem. Phys. **82**, 187 (1992).

[28] C. Leforestier, J. Phys. Chem. **94**, 9388 (1991).

[29] D. T. Colbert and H. W. Miller, J. Chem. Phys. **96**, 1982 (1992).

[30] M. Baer and H. Nakamura, J. Chem. Phys. **87**, 4651 (1987).

[31] M. Baer, H. Nakamura, and A. Ohsaki, Chem. Phys. Lett. **131**, 468 (1986).

[32] J. Echave and D. C. Clary, Chem. Phys. Lett. **190**, 225 (1992).

[33] C. Leforestier, Grid methods in atomic and molecular quantum calculations, in 4^{th} *Topsoe Summer School on Time Dependent Methods in Quantum Mechanics*, Copenhagen, 1991, G.D.Billing.

[34] D. O. Harris, G. G. Engerholm, and W. D. Gwinn, J. Chem. Phys. **43**, 1515 (1965).

[35] D. Grimbert, B. Lassier-Govers, and V. Sidis, Chem. Phys. **124**, 187 (1988).

[36] M. Monnerville and J. M. Robbe, J. Chem. Phys. **101**, 7580 (1994).

TABLE I. Convergence of positions, E, and widths, Γ, for resonances in the $H^+ + O_2$ ($\ell = 0, \gamma = 45°$) collisional system, described in the IOS approximation and using the OPM described in Sec. II and Sec. III D. The table lists results from 5 different OPM calculations with $\Delta R_{opt} = 3, 4, 5, 6$ and 7 au arranged in the 5 pairs of columns. The results are reported in atomic units and relative to the zero-point vibrational energy (3.508×10^{-3} Hartree as measured from the bottom of the potential in the entrance channel, cf. Fig. 5). As an illustration to this table see Fig. 7 where the resonance state number 10 is plotted.

Nr.	E [b]	Γ [c]	E [b]	Γ [c]	E [b]	Γ [c]	E [b]	Γ [c]	E [b]	Γ [c]
	$\Delta R_{opt} = 7$ au		$\Delta R_{opt} = 6$ au		$\Delta R_{opt} = 5$ au		$\Delta R_{opt} = 4$ au		$\Delta R_{opt} = 3$ au	
1	0.814	1.8(−3)	0.814	1.8(−3)	0.813	1.6(−3)	0.815	2.0(−2)	0.815	2.0(−2)
2	1.489	1.5(−2)	1.489	1.5(−2)	1.489	1.5(−2)	1.490	1.6(−2)	1.489	1.4(−2)
3	2.042	1.8(−1)	2.042	1.8(−1)	2.042	1.8(−1)	... [a]	... [a]	... [a]	... [a]
4	2.215	4.0(−7)	2.215	4.0(−7)	2.215	4.0(−7)	2.215	4.0(−7)	2.215	4.0(−7)
5	2.492	7.2(−1)	2.492	7.4(−1)	... [a]	... [a]	... [a]	... [a]	... [a]	... [a]
6	2.869	2.8(−4)	2.869	2.8(−4)	2.869	2.8(−4)	2.869	2.8(−4)	2.869	2.8(−4)
7	3.092	8.2(−1)	3.092	8.2(−1)	3.064	8.0(−1)	3.110	7.0(−1)	... [a]	... [a]
8	3.186	1.3(−6)	3.186	1.3(−6)	3.186	1.3(−6)	3.186	1.3(−6)	3.186	1.3(−6)
9	3.616	2.4(−1)	3.616	2.4(−1)	3.616	2.4(−1)	3.615	2.2(−1)	... [a]	... [a]
10	3.780	4.0(−2)	3.780	4.0(−2)	3.780	4.0(−2)	3.780	4.0(−2)	3.780	4.0(−2)
11	3.818	8.4(−1)	3.817	8.4(−1)	3.824	8.6(−1)	... [a]	... [a]	... [a]	... [a]
12	4.017	2.4(−4)	4.017	2.4(−4)	4.017	2.4(−4)	4.017	2.4(−4)	4.017	2.6(−4)
13	4.256	5.4(−3)	4.256	5.4(−3)	4.256	5.4(−3)	4.256	5.4(−3)	4.256	5.4(−3)
14	4.436	3.2(−2)	4.436	3.2(−2)	4.436	3.2(−2)	4.436	3.2(−2)	4.436	3.2(−2)
15	4.665	3.4(−2)	4.665	3.4(−2)	4.665	3.4(−2)	4.665	3.4(−2)	4.665	3.4(−2)
16	4.707	1.3(−2)	4.707	1.3(−2)	4.707	1.3(−2)	4.707	1.3(−2)	4.707	1.3(−2)
17	5.144	1.3(−2)	5.144	1.3(−2)	5.144	1.3(−2)	5.144	1.3(−2)	5.144	1.3(−2)
18	5.416	1.1(−2)	5.416	1.1(−2)	5.416	1.1(−2)	5.416	1.1(−2)	5.416	1.1(−2)

19	5.910	3.2(−2)	5.910	3.2(−2)	5.910	3.2(−2)	5.910	3.2(−2)	5.910	3.2(−2)
20	5.965	1.3(−4)	5.965	1.3(−4)	5.965	1.3(−4)	5.965	1.3(−4)	5.965	1.3(−4)
21	6.096	1.2(−2)	6.095	1.2(−2)	6.094	1.2(−2)	6.082	1.2(−2)	... [a]	... [a]
22	6.358	6.8(−2)	6.358	6.8(−2)	6.358	6.8(−2)	6.358	6.8(−2)	6.358	6.8(−2)
23	6.464	1.6(−3)	6.464	1.6(−3)	6.464	1.6(−3)	6.464	1.6(−3)	6.464	1.6(−3)
24	6.660	4.6(−2)	6.660	4.6(−2)	6.660	4.6(−2)	6.660	4.6(−2)	6.660	4.6(−2)
25	6.856	7.4(−2)	6.856	6.6(−2)	6.856	6.2(−2)	6.856	6.0(−2)	6.856	6.0(−2)

[a]Difficult to assign, i.e. no clear stagnation-point was found for this particular choice of the optical potential.

[b]The positions of the resonances are listed in units of 10^{-3} Hartree.

[c]The width of the resonances are listed in units of 10^{-3} au. We have further used the short notation $(-x)$ for 10^{-x}, i.e. a value of e.g. $8.4(-1)$ correspond to a width of 8.4×10^{-4}au.

TABLE II. Comparison of positions, E, widths, Γ, and lifetimes, τ, for resonances in the $H^+ + O_2(\ell = 0, \gamma = 45°)$ collisional system, described in the IOS approximation. The first three columns correspond to the converted results from Table I obtained using the optical potential method. The last three columns correspond to previous results found by Grimbert *et al.* [2] solving the closed coupled set of equations. The results are reported in atomic units and relative to the zero-point vibrational energy (3.508×10^{-3} Hartree as measured from the bottom of the potential in the entrance channel, cf. Fig. 5).

	Optical potential method			Solving coupled equations [2]		
Nr.	E (10^{-3} au)	Γ (10^{-3} au) [c]	τ (s) [c]	E (10^{-3} au)	Γ (10^{-3} au) [c]	τ (s) [c]
1	0.81	1.8(−3) [b]	1.3(−11) [b]	0.80	1.4(−3)	1.7(−11)
2	1.49	1.5(−2)	1.6(−12)	1.49	5.8(−3)	4.1(−12)
3	2.04	1.8(−1)	1.3(−13)	1.85	1.2(−1)	1.9(−13)
4	2.22	4.0(−7)	6.0(−8)	... [a]	... [a]	... [a]
5	2.49 [b]	7(−1) [b]	3(−14) [b]	2.36	8.6(−2)	2.8(−13)
6	2.87	2.8(−4)	8.6(−11)	... [a]	... [a]	... [a]
7	3.01	8.2(−1) [b]	2.9(−14) [b]	2.93	1.3(−2)	1.8(−12)
8	3.19	1.3(−6)	1.9(−8)	... [a]	... [a]	... [a]
9	3.62	2.4(−1)	1.0(−13)	3.72	1.9(−1)	1.3(−13)
10	3.78	4.0(−2)	6.0(−13)	3.89	1.5(−3)	1.7(−11)
11	3.82 [b]	8.4(−1) [b]	2.9(−14) [b]	3.99	1.3(−1)	1.9(−13)
12	4.02	2.4(−4)	1.0(−10)	... [a]	... [a]	... [a]
13	4.26	5.4(−3)	4.5(−12)	... [a]	... [a]	... [a]
14	4.44	3.2(−2)	7.6(−13)	... [a]	... [a]	... [a]
15	4.67	3.4(−2)	7.1(−13)	4.55	4.8(−2)	5.0(−13)
16	4.71	1.3(−2)	1.9(−12)	5.08	7.5(−3)	3.2(−12)
17	5.14	1.3(−2)	1.9(−12)	5.21	4.1(−2)	6.0(−13)
18	5.42	1.1(−2)	2.2(−12)	5.58	1.4(−2)	1.7(−12)

19	5.91	3.2(−2)	7.6(−13)	5.87	6.8(−3)	3.5(−12)
20	5.97	1.3(−4)	1.9(−10)	... [a]	... [a]	... [a]
21	6.09	1.2(−2)	2.0(−12)	6.04	3.1(−2)	8.0(−13)
22	6.36	6.8(−2)	3.6(−13)	6.44	6.5(−2)	3.7(−13)
23	6.46	1.6(−3)	1.5(−11)	6.70	5.8(−3)	4.1(−12)
24	6.66	4.6(−2)	5.3(−13)	6.81	5.2(−2)	4.7(−13)
25	6.86	7(−2) [b]	3(−13) [b]	6.95	7.4(−2)	3.3(−13)

[a]No previous resonance reported in Ref. [2].

[b]Difficult to assign, see Table I.

[c]In this column we have used the short notation $(-x)$ for 10^{-x}.